How to focus an attosecond pulse

Charles Bourassin-Bouchet, Matthias Maximilian Mang, Franck Delmotte, Pierre Chavel, Sébastien de Rossi

How to focus an attosecond pulse

C. Bourassin-Bouchet,[1,2,*] **M. M. Mang,**[2] **F. Delmotte,**[1] **P. Chavel,**[1] **and S. de Rossi**[1]

[1]*Laboratoire Charles Fabry, Institut d'Optique, CNRS, Univ Paris-Sud, 2 avenue Augustin Fresnel, 91127 Palaiseau Cedex, France*

[2]*Clarendon Laboratory, University of Oxford, Parks Road, Oxford, OX1 3PU, United Kingdom*

[*]*charles.bourassin-bouchet@institutoptique.fr*

Abstract: Attosecond experiments involving focusing of attosecond light pulses can suffer from a spread of the attosecond radiation both in space and time due to optical aberrations. We present a detailed numerical study of the distortions induced in the most common focusing geometries that make use of parabolic, spherical, toroidal and ellipsoidal mirrors. We deduce the consequences on the pulse duration and possible issues that could arise in applications of attosecond pulses. This should serve as a guideline for setting up attosecond focusing optics.

OCIS codes: (340.7480) X-rays, soft x-rays, extreme ultraviolet (EUV); (320.5550) Pulses; (080.1010) Aberrations (global).

References and links

1. M. Hentschel, R. Kienberger, Ch. Spielmann, G. A. Reider, N. Milosevic, T. Brabec, P. Corkum, U. Heinzmann, M. Drescher, and F. Krausz, "Attosecond metrology," Nature (London) **414,** 509–513 (2001).
2. P. M. Paul, E. S. Toma, P. Breger, G. Mullot, F. Augé, Ph. Balcou, H. G. Muller, and P. Agostini, "Observation of a Train of Attosecond Pulses from High Harmonic Generation," Science **292,** 1689–1692 (2001).
3. J. Itatani, J. Levesque, D. Zeidler, H. Niikura, H. Pépin, J. C. Kieffer, P. B. Corkum, and D. M. Villeneuve, "Tomographic imaging of molecular orbitals," Nature (London) **432,** 867–871 (2004).
4. D. Shafir, H. Soifer, B. D. Bruner, M. Dagan, Y. Mairesse, S. Patchkovskii, M. Y. Ivanov, O. Smirnova, and N. Dudovich, "Resolving the time when an electron exits a tunnelling barrier," Nature (London) **485,** 343–346 (2012).
5. Y. Mairesse, A. de Bohan, L. J. Frasinski, H. Merdji, L. C. Dinu, P. Monchicourt, P. Breger, M. Kovačev, R. Taïeb, B. Carré, H. G. Muller, P. Agostini, and P. Salières, "Attosecond synchronization of high-harmonic soft x-rays," Science **302,** 1540–1543 (2003).
6. E. Goulielmakis, M. Schultze, M. Hofstetter, V. S. Yakovlev, J. Gagnon, M. Uiberacker, A. L. Aquila, E. M. Gullikson, D. T. Attwood, R. Kienberger, F. Krausz, and U. Kleineberg, "Single-Cycle Nonlinear Optics," Science **320,** 1614–1617 (2008).
7. T. Sekikawa, A. Kosuge, T. Kanai, and S. Watanabe, "Nonlinear optics in the extreme ultraviolet," Nature (London) **432,** 605–608 (2004).
8. A. L. Cavalieri, N. Müller, Th. Uphues, V. S. Yakovlev, A. Baltŭska, B. Horvath, B. Schmidt, L. Blümel, R. Holzwarth, S. Hendel, M. Drescher, U. Kleineberg, P. M. Echenique, R. Kienberger, F. Krausz, and U. Heinzmann, "Attosecond spectroscopy in condensed matter," Nature (London) **449,** 1029–1032 (2007).
9. M. Schultze, M. Fieß, N. Karpowicz, J. Gagnon, M. Korbman, M. Hofstetter, S. Neppl, A. L. Cavalieri, Y. Komninos, Th. Mercouris, C. A. Nicolaides, R. Pazourek, S. Nagele, J. Feist, J. Burgdörfer, A. M. Azzeer, R. Ernstorfer, R. Kienberger, U. Kleineberg, E. Goulielmakis, F. Krausz, and V. S. Yakovlev, "Delay in Photoemission," Science **328,** 1658–1662 (2010).
10. G. Sansone, E. Benedetti, F. Calegari, C. Vozzi, L. Avaldi, R. Flammini, L. Poletto, P. Villoresi, C. Altucci, R. Velotta, S. Stagira, S. De Silvestri, and M. Nisoli, "Isolated Single-Cycle Attosecond Pulses," Science **314,** 443–446 (2006).
11. M. Born and E. Wolf, *Principles of Optics* 7th ed. (Pergamon, London, 1999).
12. S. Akturk, X. Gu, P. Bowlan, and R. Trebino, "Spatio-temporal couplings in ultrashort laser pulses," J. Opt. **12,** 093001 (2010).

#179798 - $15.00 USD Received 13 Nov 2012; revised 21 Dec 2012; accepted 27 Dec 2012; published 25 Jan 2013

13. Z. Bor, "Distortion of femtosecond laser pulses in lenses," Opt. Lett. **14,** 119–121 (1989).
14. M. Kempe, and W. Rudolph, "Femtosecond pulses in the focal region of lenses," Phys. Rev. A **48,** 4721–4729 (1993).
15. U. Fuchs, U. Zeitner, and A. Tünnermann, "Ultra-short pulse propagation in complex optical systems," Opt. Express **13,** 3852–3861 (2005).
16. C. Bourassin-Bouchet, S. de Rossi, F. Delmotte, and P. Chavel, "Spatiotemporal distortions of attosecond pulses," J. Opt. Soc. Am. A **27,** 1395–1403 (2010).
17. P. Salières, A. L'Huillier, and M. Lewenstein, "Coherence control of high-order harmonics," Phys. Rev. Lett. **74,** 3776–3779 (1995).
18. M. Kempe, U. Stamm, B. Wilhelmi, and W. Rudolph, "Spatial and temporal transformation of femtosecond laser pulses by lenses and lens systems," J. Opt. Soc. Am. B **9,** 1158–1165 (1992).
19. C. Bourassin-Bouchet, M. Stephens, S. de Rossi, F. Delmotte, and P. Chavel, "Duration of ultrashort pulses in the presence of spatio-temporal coupling," Opt. Express **19,** 17357–17371 (2011).
20. A. Ravasio, D. Gauthier, F. R. N. C. Maia, M. Billon, J-P. Caumes, D. Garzella, M. Géléoc, O. Gobert, J-F. Hergott, A-M. Pena, H. Perez, B. Carré, E. Bourhis, J. Gierak, A. Madouri, D. Mailly, B. Schiedt, M. Fajardo, J. Gautier, P. Zeitoun, P. H. Bucksbaum, J. Hajdu, and H. Merdji, "Single-Shot Diffractive Imaging with a Table-Top Femtosecond Soft X-Ray Laser-Harmonics Source," Phys. Rev. Lett. **103,** 028104 (2009).
21. Y. Ménesguen, S. de Rossi, E. Meltchakov, and F. Delmotte, "Aperiodic multilayer mirrors for efficient broadband reflection in the extreme ultraviolet," Appl. Phys. A **98,** 305–309 (2010).

1. Introduction

Attosecond light pulses in the extreme ultraviolet (XUV) range have been a very active research field since their first observation in 2001 [1, 2]. Such pulses can be generated by the interaction between an intense femtosecond laser pulse and a gaseous or solid target. This process is known as high harmonic generation and has led to a variety of experiments in the past ten years. On one hand there are the so-called *in situ* experiments which first consist in changing the conditions of the interaction in the generation medium. This is then followed by a lensless measurement in order to observe the changes of the light properties in the far field [3, 4]. On the other hand, attosecond pulses can be used to probe another medium. The induced interaction enables one to characterise the temporal profile of the attosecond emission [5, 6], to study nonlinear XUV processes [7] or to perform electronic spectroscopy [8, 9]. In all these cases, focusing the attosecond radiation onto the target is a compulsory requirement. This is generally fulfilled by using a near-normal incidence spherical multilayer mirror [1, 6, 8, 9] or a grazing incidence toroidal mirror [2, 5, 10].

However, as all focusing optics, these mirrors can induce geometric aberrations, that is defaults on the focused beam due to the geometric shape of the mirror. Usually such aberrations are studied in the case of monochromatic beams [11] regarding the distortions that they induce on the focal spot shape, and thus on the resolution of imaging systems. However, when used to focus broadband ultrashort radiation, aberrations can have an impact on the spatio-temporal shape of the light pulse as well. More precisely, they can lead to so-called space-time coupling [12], that means that the pulse profile is spatially dependent. This can dramatically deteriorate the shape of the beam and strongly increase the pulse duration at the focus. Both effects can significantly compromise the quality of data obtained in such experiments. Such phenomena have been fully studied in the case of visible-IR femtosecond pulses [13–15]. This becomes even more critical in the attosecond regime as shown in a previous article [16]. However, this study was based only on diffraction theory in the specific cases of attosecond pulses reflected off near normal incidence parabolic and spherical multilayer mirrors.

In this paper, we present a full study of the distortions induced by focusing optics on attosecond light pulses. First, we describe the three tools used for our analysis, namely a fully geometric approach, a diffractive approach, and an approach based on the study of the duration of aberrated pulses. Each of these tools allows one to make distinct and complementary conclusions. Second, we study a variety of focusing geometries covering the full range of optics used

#179798 - $15.00 USD Received 13 Nov 2012; revised 21 Dec 2012; accepted 27 Dec 2012; published 25 Jan 2013

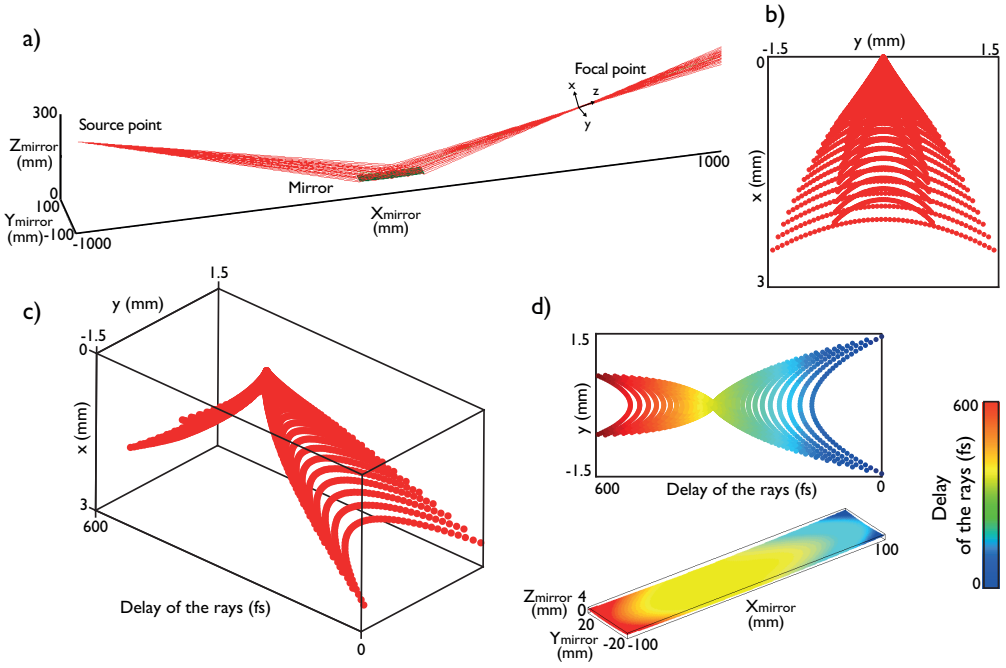

Fig. 1. Description of the geometric approach (a) Geometrical rays are reflected off a grazing incidence toroidal mirror and recombine in the focal point. (b) 2D spot diagram, calculated in a plane perpendicular to the optical axis. (c) Corresponding 3D spot diagram. (d) 3D spot diagram seen from above along with the surface of the mirror. The colormap represents the relative delay between the rays.

to focus attosecond pulses, i.e. toroidal, spherical, parabolic and ellipsoidal mirrors. Finally, we conclude on the consequences of the induced distortions on the pulse duration.

2. Approaches of the problem

Aberrations arise from variations of optical path lengths across the beam. Equivalently, these path lengths variations can be considered as elementary time delays between different points in the beam. Thus a logical starting point is to evaluate the arrival times across the pulse at the focal plane.

2.1. Geometric approach

In order to simulate the change in path lengths in the focal spot induced by attosecond optics, we performed ray-tracing calculations. We illustrate our approach in Fig. 1 by considering the case of a toroidal mirror. This mirror has a focal length of 375 mm for a grazing angle of 15°, and a size of 200×40 mm. The mirror is used with a magnification of 0.6, so that the distance between the source and the mirror equals 1 m, and the one between the mirror and the paraxial focus equals 600 mm. Rays are emitted by a point source and hit the mirror surface in an equally spaced manner, see Fig. 1(a). The focusing quality can be visualized by mapping the cross-section of the individual rays onto a plane perpendicular to the optical axis, as shown in Fig. 1(b). However, such a spot diagram only provides information about the shape of the focal spot, and not about the change in optical path lengths.

#179798 - $15.00 USD Received 13 Nov 2012; revised 21 Dec 2012; accepted 27 Dec 2012; published 25 Jan 2013

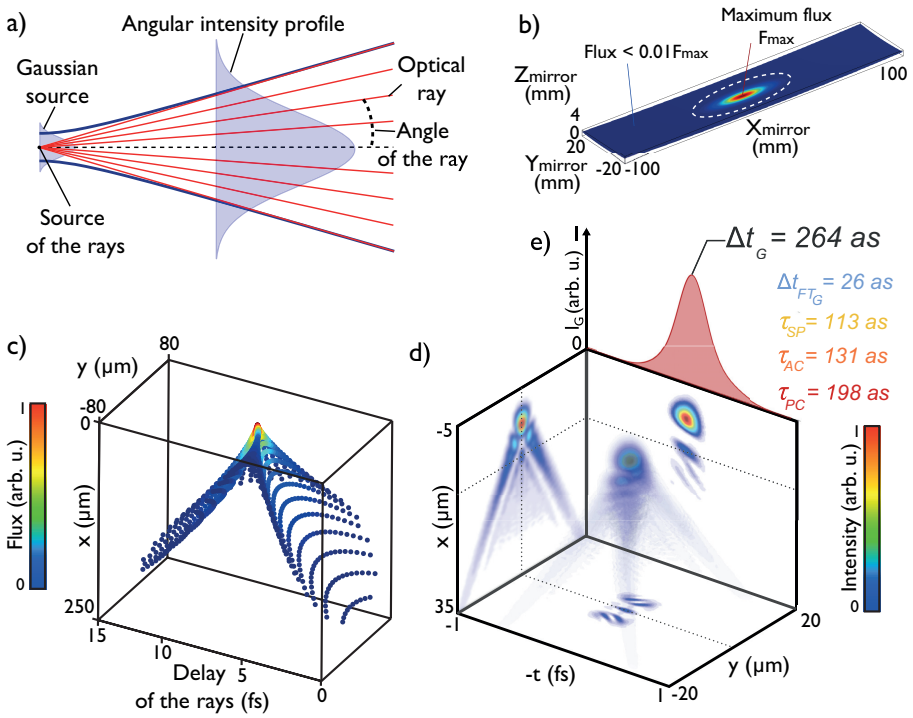

Fig. 2. (a) Principle of the simulation of the gaussian source with the ray-tracing. (b) Resulting spectrally integrated gaussian flux distribution on the mirror surface. (c) 3D spot diagram obtained if taking into account the flux distribution on the mirror. (d) Spatio-temporal intensity distribution obtained by the diffractive approach. The projections on the (x,t) and (y,t) sides of the box stand for two slices of the 3D pulse located on the dashed lines. The projection on the (x,y) side corresponds to the temporally integrated pulse, that is the image that should be obtained if using a CCD sensor. (e) The spatially integrated pulse $I_G(t)$ associated to the spatio-temporal pulse is depicted above the box along with its global duration Δt_G and the decomposition of the latter into the four durations.

As the path length of each ray from the source to the spot diagram plane is known, this can be converted into a temporal delay of the rays with respect to each other. By adding this temporal dimension to the usual 2D spot diagram, one obtains a 3D spot diagram (see Fig. 1(c)) representing the spatio-temporal shape of the focused pulse.

As it becomes apparent in Fig. 1(b-c), a grazing incidence toroidal mirror introduces coma to the beam in the chosen geometry, manifested by the typical tail-shape of the focal spot. In addition, the spatio-temporal shape appears to be composed of two different bunches of rays with either short or longer path lengths, corresponding to two different groups of arrival times. From Fig. 1(d), it can be understood that the long path lengths correspond to rays reflected off the side of the mirror closer to the source while the short path lengths are generated by reflection off the opposite side. The maximum time delay between rays is as large as 600 fs, which exceeds the attosecond timescale by several orders of magnitude.

However, the flux coming from the edges of the mirror is in general much weaker than the flux from the centre. In order to simulate a more realistic scenario, we assume that the attosecond source emits a beam with a gaussian profile [17]. As described in Fig. 2(a) and in Ref. [16], a gaussian beam can be represented as a punctual source emitting rays of light with

#179798 - $15.00 USD Received 13 Nov 2012; revised 21 Dec 2012; accepted 27 Dec 2012; published 25 Jan 2013

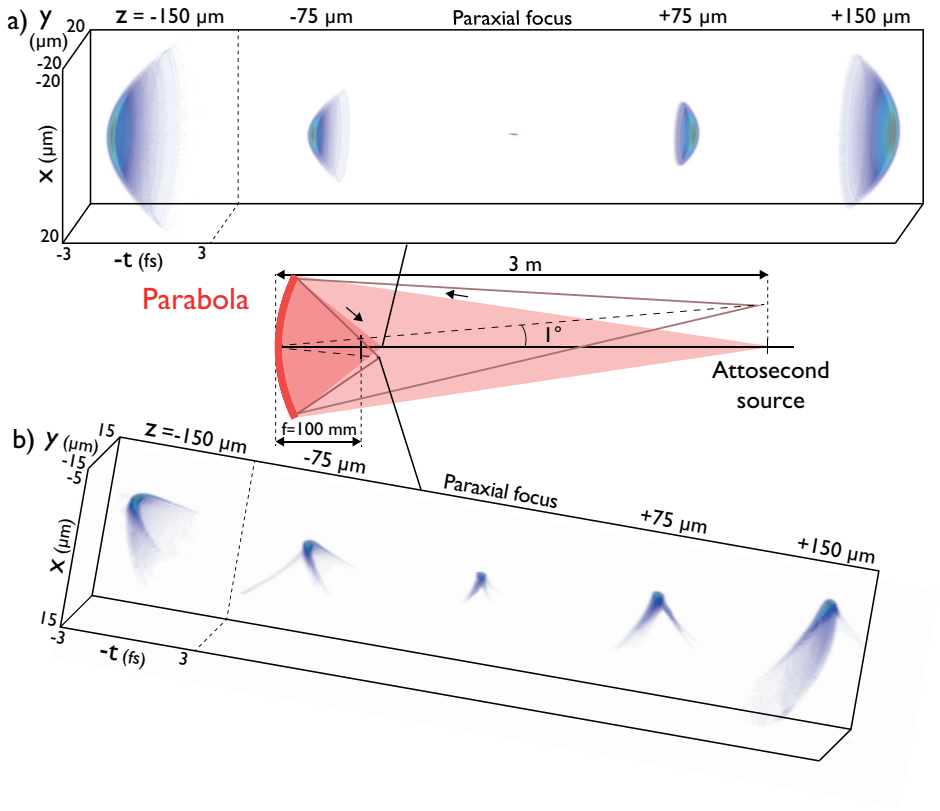

Fig. 3. Spatio-temporal evolution of an attosecond pulse focused by a parabola. Central panel: description of the two focusing geometries. (a) (resp. (b)) Evolution of the (x,y,t) intensity distribution of the attosecond pulse along the z axis near the paraxial focus when considering a 0° (resp. 1°) field angle.

an angularly gaussian intensity profile as long as one remains far from the Rayleigh range. Therefore, once the beam divergence and the wavelength are set, one can attribute an intensity value to each optical ray emitted by the punctual source. One can then deduce the distribution of light on the mirror surface for each wavelength, as shown in Fig. 2(b). In that case, the chosen spectrum is gaussian centered at 75 eV with a full width at half maximum (FWHM) of 30 eV and the beam divergence equals 6 mrad FWHM at 75 eV. It becomes clear that the flux is negligible on the major part of the mirror. Thus for all following analysis, we only take into account rays carrying a flux larger than 1% of the maximum flux F_{max}, that is the rays impacting the inner part of the white dashed circle in Fig. 2(b). Consequently, the maximum time delay between rays has decreased to 15 fs, as shown in Fig. 2(c). The majority of the flux is now concentrated at the peak of the coma-tail.

2.2. *Diffractive approach*

The geometric approach is a useful tool to gain insight into the spatio-temporal shape of the pulse. However, it does not provide information about the electric field around the focus. In order to take into account effects arising from wave optics, we include diffractive calculations to our ray tracing simulations.

#179798 - $15.00 USD Received 13 Nov 2012; revised 21 Dec 2012; accepted 27 Dec 2012; published 25 Jan 2013

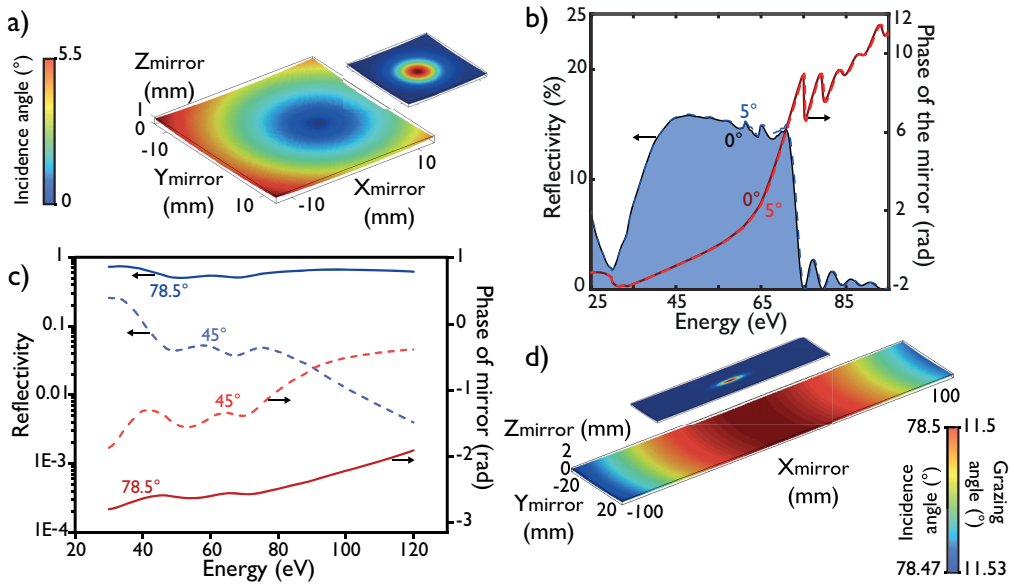

Fig. 4. Evolution of the angle of incidence of the rays (main pannel) and of the polychromatic flux (smaller panel), at the surface of (a) a focusing multilayer mirror for a 1° field angle, and of (d) a toroidal mirror in a $2f-2f$ geometry for a grazing angle of 11.5°. (b) Reflectivity and phase of the broadband multilayer mirror described in Ref. [21] for an angle of incidence of 0° and 5°. (c) Reflectivity and phase of a platinum mirror for an angle of incidence of 78.5°, that is a grazing angle of 11.5°, and of 45°.

The general idea is that at distances from the focal point that are large compared to the focal length, the rays are strongly angularly spread. Therefore they do not interfere with each other. Diffraction effects are then negligible, and the pulse can be correctly described by geometric optics. In addition to the gaussian spatial profile, we first add an elementary electric field, i.e. a spectrum and a spectral phase, to each ray emitted by the source. It is important to notice that the initial pulse at the source exhibits no spatio-temporal distortions. After reflection off the mirror, we deduce the electric field distribution at the intersection of the rays with a plane where the beam is highly defocused. From here, we then propagate the field back to the focal point by using the diffraction formula of Rayleigh-Sommerfeld [11]. The overall procedure is described in more detail in Ref. [16]. Comparing the results with the geometric approach, as shown in Fig. 2(c-d), reveals that the overall shape is preserved, notably the tail-shape and the two groups of arrival times that are characteristic for coma. In addition, the diffractive calculations reveal more details about the pulse shape such as interference effects. These features were hidden in the geometric approach.

2.3. Space-time coupling and duration of aberrated pulses

The first two methods give a detailed description of the three dimensional pulse shape at the focus. Since they describe the picture of the pulse in a more qualitative way, we now try to study the strength of the aberrations by estimating a pulse duration. In that scope, we first spatially integrate the 3D set of data, see Fig. 2(e). It thus becomes possible to calculate a global duration of the resulting temporal signal [12, 18]. This duration will increase under the influence of space-time coupling.

#179798 - $15.00 USD Received 13 Nov 2012; revised 21 Dec 2012; accepted 27 Dec 2012; published 25 Jan 2013

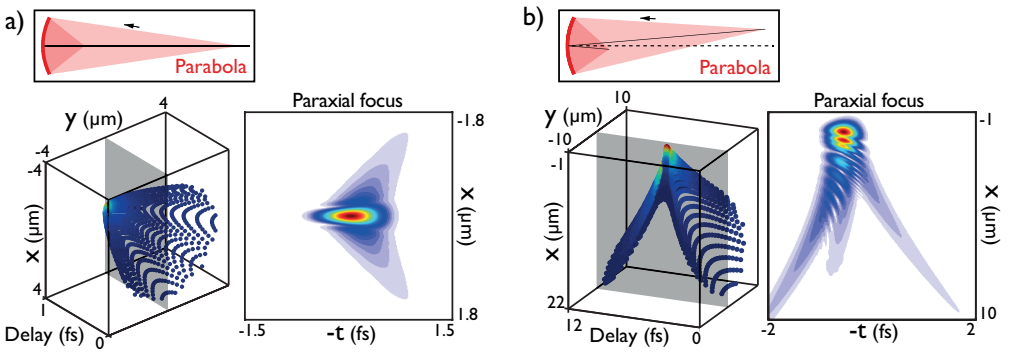

Fig. 5. Detailed evolution of a pulse focused by a parabola in the case (a) (resp. (b)) of 0° (resp. 1°) field angle. Upper panel: studied focusing geometry. Left panel: 3D spot diagram. Right panel: evolution of the modulus of the electric field in the $y = 0$ plane, shaded in grey on the 3D spot diagrams.

In mathematical terms, a pulse is said to exhibit space-time coupling if the spatio-temporal profile of the electric field cannot be represented as a product of a purely spatial function $g(x,y)$ and a function depending only on time, or equivalently on frequency $f(\omega)$, see Eq. (1):

$$E(x,y,\omega) \neq f(\omega)\cdot g(x,y) = |f(\omega)||g(x,y)|\cdot \exp\left[i\Psi(x,y)+i\Phi(\omega)\right]. \tag{1}$$

According to the approach used in Ref. [19], the global duration Δt_G of an arbitrarily complex pulse, defined as the RMS duration of the spatially integrated pulse $I_G(t)$, can always be decomposed into different contributions:

$$\Delta t_G^2 = \Delta t_{FT_G}^2 + \tau_{SP}^2 + \tau_{AC}^2 + \tau_{PC}^2 \tag{2}$$

The different terms in Eq. (2) have the following meaning:

i) Δt_{FT_G} is the global Fourier Transform limit of the pulse. For a given spectrum, this duration corresponds to the shortest possible pulse duration, which in the example depicted in Fig. 2(e) equals 26 *as*. It is reached when no space-time coupling is present and the spectral phase is linear.

ii) τ_{SP}, determined by the *spectral phase*, represents the pulse stretch induced by phenomena such as temporal chirp or higher-order dispersion.

iii) *Amplitude coupling*, represented by τ_{AC}, is present when $|E(x,y,\omega)|$ cannot be written as $|f(\omega)||g(x,y)|$, that is when the spectrum depends on space.

iv) *Phase coupling*, represented by τ_{PC}, is present when the phase of $E(x,y,\omega)$ cannot be expressed as $\Psi(x,y)+\Phi(\omega)$. This is equivalent to saying that the group delay, which is the derivative of the phase with respect to ω, is not only dependent on frequency.

One asset of Eq. (2) is that it is very general. It can be applied to aberrated pulses obtained via the diffractive approach in any focusing geometry.

#179798 - $15.00 USD Received 13 Nov 2012; revised 21 Dec 2012; accepted 27 Dec 2012; published 25 Jan 2013

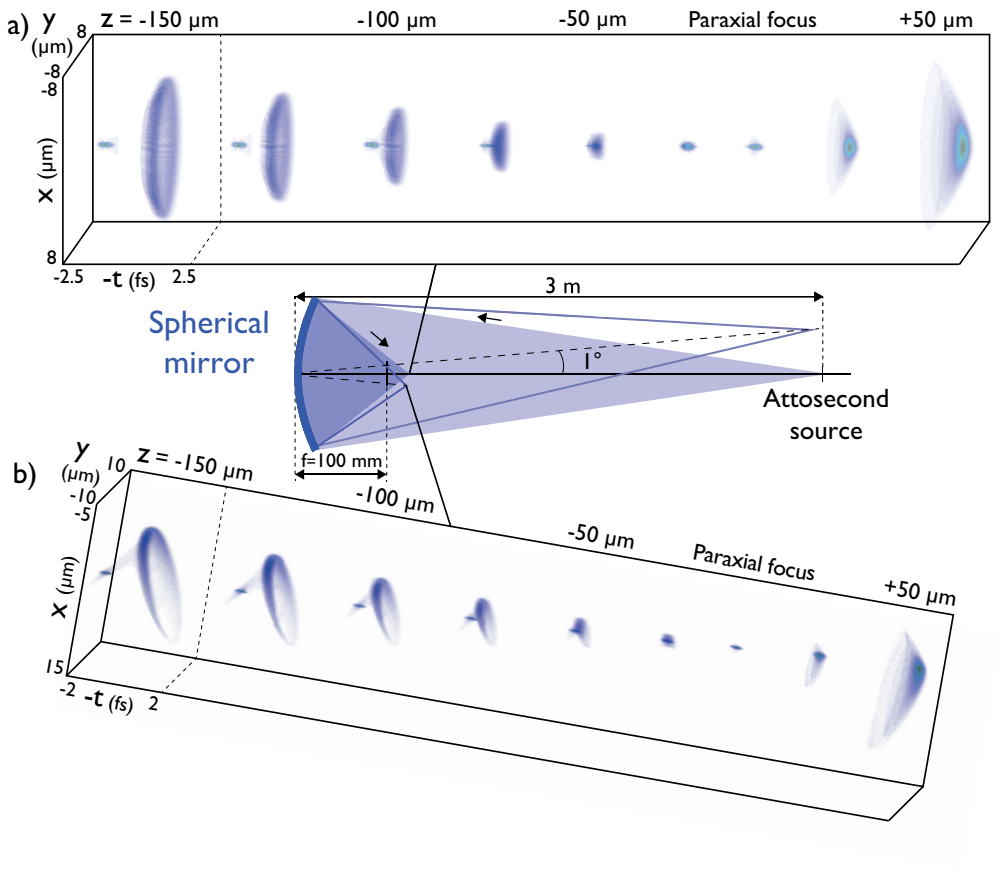

Fig. 6. Spatio-temporal evolution of an attosecond pulse focused by a spherical mirror. Central panel: description of the two focusing geometries. (a) (resp. (b)) Evolution of the (x,y,t) intensity distribution of the attosecond pulse along the z axis near the paraxial focus when considering a 0° (resp. 1°) field angle.

3. Simulation of various focusing geometries

There are mainly two ways to focus an attosecond pulse: near-normal incidence multilayer mirrors and grazing incidence mirrors. Thus we simulate the pulses focused by both of these categories. In order to compare the different focusing geometries, we use the same initial conditions for all the following simulations. More precisely, we consider a gaussian XUV spectrum centered at 75 eV with a full width at half maximum of 30 eV. A group delay dispersion of 6000 as^2/rad is also added to simulate the attochirp [5]. The resulting pulse duration at the source is 118 as RMS, 277 as FWHM. The attosecond source emits a gaussian beam, the angular profile of which has a FWHM of 3 mrad at 75 eV (5.3 mrad full width at $1/e^2$).

3.1. Parabola and spherical mirror

We first consider the case of a parabola. This optic is mainly used to focus collimated beams, but can also be used to focus beams emitted from a source at a finite distance [20]. We choose to consider the latter case. As depicted in Fig. 3, the chosen focal length f equals 100 mm, and the mirror diameter equals one inch. The attosecond source is placed 3 m away from the mirror

#179798 - $15.00 USD Received 13 Nov 2012; revised 21 Dec 2012; accepted 27 Dec 2012; published 25 Jan 2013

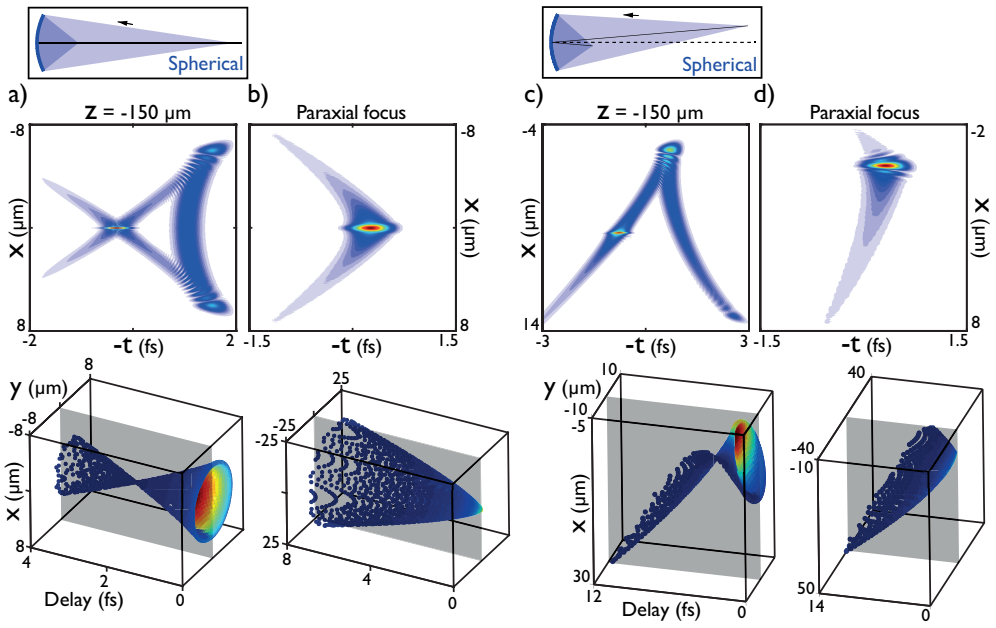

Fig. 7. Detailed evolution of a pulse focused by a spherical mirror. Upper panel: studied focusing geometry. Central panel (resp. lower panel): evolution of the modulus of the electric field in the $y = 0$ plane (resp. of the corresponding 3D spot diagram), 150 μm before the paraxial focus (a-c) and at the focus (b-d) when considering a 0° (a-b) and 1° field angle (c-d). The shaded plane on the 3D spot diagrams indicates the $y = 0$ plane.

with a field angle of 0° or 1°. It is important to check that the response of the multilayer coating will remain homogeneous throughout the mirror surface. Indeed, the complex reflectivity of a multilayer stack depends on the angle of incidence of the beam that can slightly vary locally. As shown in Fig. 4(a) in these geometries, the angle of incidence of the rays on the mirror can vary from 0° to 5.5°. If considering a realistic broadband coating suitable for attosecond pulses [21], it turns out that neither the reflectivity nor the phase of the mirror will be affected by such a small deviation of the angle of incidence, see Fig. 4(b). Therefore, one can neglect the influence of the coating, and we now consider that only the geometric shape of the substrate will have an influence on the focused pulse.

First, the source is placed on the mirror axis, i.e. at 0° field angle. Figure 3(a) represents the spatio-temporal evolution of the pulse intensity in this geometry. The pulse appears to be nicely focused. However, as revealed by a geometric study in Fig. 5(a), the delays of the rays across the beam can vary up to 1 fs. We therefore expect some visible distortions of the attosecond structure. This is confirmed by the diffractive approach in Fig. 5(a). Here, in order to emphasize the underlying structure of the pulse, we plot the modulus of the attosecond electric field instead of its intensity. One can see two wings arriving before the core of the pulse. The origin of these delays comes from the residual spherical aberration in this geometry. Indeed, a parabola will be rigorously stigmatic if the source is moved to infinity. We now consider that the geometry has a 1° field angle. As shown in Fig. 3(b), the shape of the pulses looses its symmetry of revolution around the propagation axis. At short distances around the focus, a double pulse front appears. As seen in Section 2, this can be attributed to coma aberration. Moreover, the detailed evolution described in Fig. 5(b) reveals strong interferences at the crossing of the two pulse fronts, which

#179798 - $15.00 USD Received 13 Nov 2012; revised 21 Dec 2012; accepted 27 Dec 2012; published 25 Jan 2013

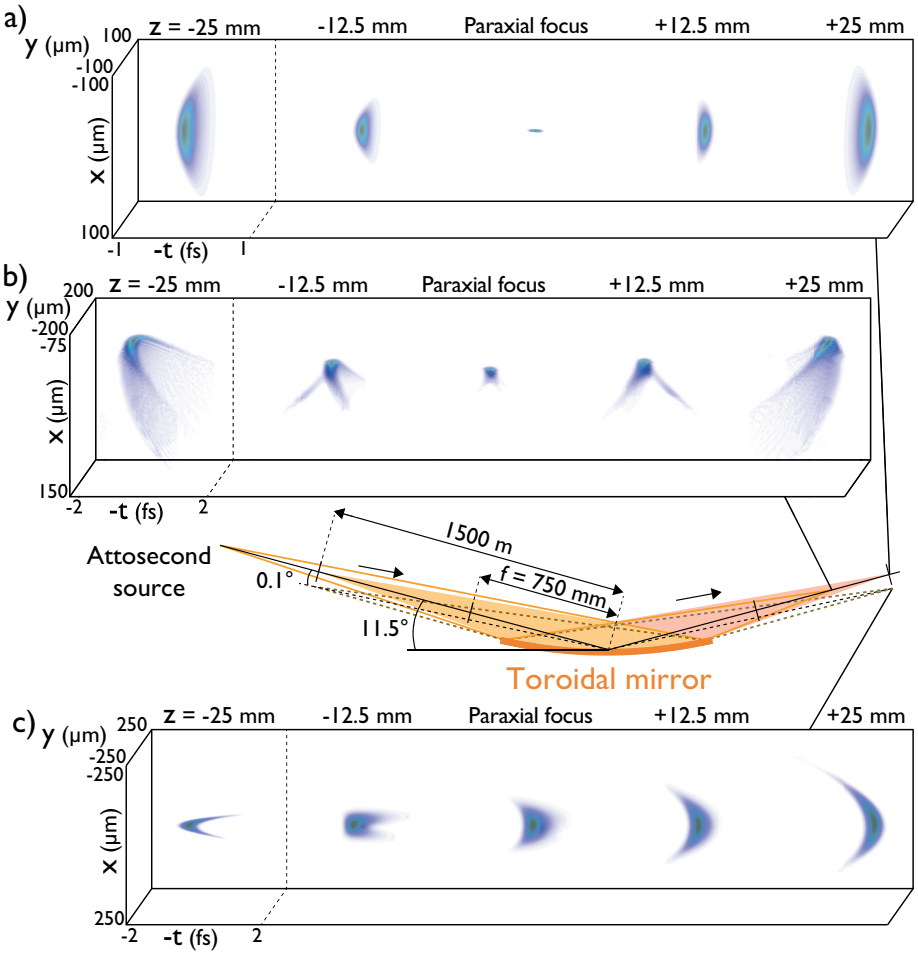

Fig. 8. **Spatio-temporal evolution of an attosecond pulse focused by a toroidal mirror.** Central panel: description of the three focusing geometries. (a-c) Evolution of the (x,y,z,t) intensity distribution of the attosecond pulse near the paraxial focus when considering (a) a magnification of 1 ($2f-2f$ geometry), (b) a magnification of 0.5, and (c) a $2f-2f$ geometry with an error of 0.1° on the grazing angle.

was hidden in the 3D spot diagram. This highlights the importance of combining the diffractive and geometric approaches.

As a next step, we study the aberrations induced by a spherical mirror used in the same focusing geometries as above. Figure 6 shows some striking differences compared to the parabolic mirror. In both geometries of 0° and 1° field angles, the main pulse front is followed by an isolated pulse before the paraxial focus. After the focus however, only one spherical pulse front is visible. A basic explanation can be found using the geometric approach. Rays reflected off the centre of the mirror carry the maximum flux, and thus correspond to the red spots on the spot diagrams of Fig. 7. Rays reflected off the edges of the mirror carry a weak flux and are represented by the blue points in the spot diagrams. It clearly appears that the latter rays are delayed with respect to the ones reflected off the centre of the mirror. They experience longer optical paths due to the spherical shape of the mirror. Before the paraxial focus, these delayed

#179798 - $15.00 USD Received 13 Nov 2012; revised 21 Dec 2012; accepted 27 Dec 2012; published 25 Jan 2013

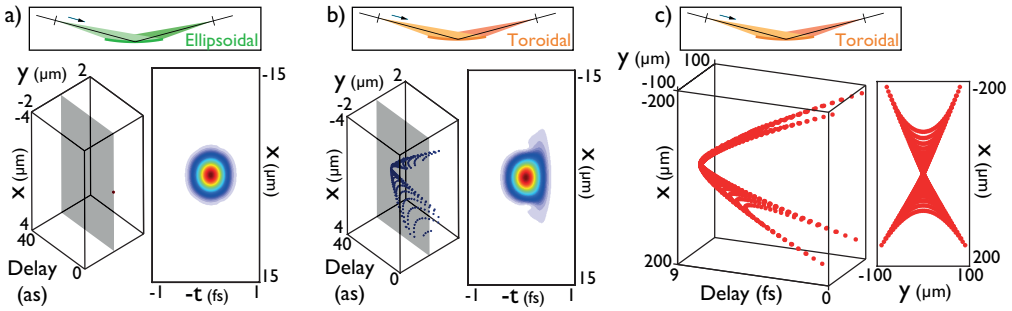

Fig. 9. Diffractive and geometric structures of pulses focused by toroidal and ellipsoidal mirrors in a $2f-2f$ geometry. Upper panels: description of the focusing geometry. (a-b) Evolution of the 3D spot diagrams (left) and of the modulus of the electric field in the $y=0$ plane (right) at the paraxial focus, in the case of (a) an ellipsoidal and (b) toroidal mirror. The shaded plane on the 3D spot diagrams at the paraxial focus indicates the $y=0$ plane. (c) 3D spot diagram at the paraxial focus of the toroidal mirror if considering the rays reflected off the full surface of the mirror.

rays are focused behind the main spherical front. This leads to the creation of an intense pulse visible in the diffractive calculation in Fig. 7(a) and 7(c). This turns out to be the most intense area of the whole pulse, a feature not accessible in the geometric approach. On the contrary, at the paraxial focus these rays diverge quickly while the rays coming from the center of the mirror are properly focused, as indicated in Fig. 7(b) and 7(d). In the case of a 1° field angle, the typical double pulse front induced by coma is superimposed to the evolution occurring at 0°. This coma aberration increases with the field angle. However for larger angles, astigmatism becomes the dominant aberration.

3.2. Toroidal and ellipsoidal mirrors

Grazing incidence mirrors constitute the other well spread category of optics used to focus attosecond pulses. These grazing mirrors are usually chosen to have a toroidal shape. We consider a toroidal mirror with a size of 200×40 mm, a focal length of 750 mm, an optimal grazing angle of 11.5° and radii of curvature equal to 7225 mm and 299 mm. In Fig. 8, we study three different geometries: the $2f-2f$ geometry, that is a magnification of 1, a magnification of 0.5, and the $2f-2f$ geometry with a 0.1° misalignment of the grazing angle.

As in the case of near-normal incidence multilayer mirrors, we first study the impact of the coating on the pulses reflected off the toroidal mirror. Due to total reflection, grazing incidence mirrors always exhibit a high and flat reflectivity and a linear spectral phase, as shown in Fig. 4(c) in the case of a platinum coated toroidal mirror in the $2f-2f$ geometry. Moreover, the variation of the incidence angle of the rays on the mirror surface is by far too small to induce any changes of the coating response in space. Therefore, the influence of the coating on the reflected pulses can be neglected.

The $2f-2f$ geometry appears to nicely focus the pulse. In order to check the quality of this focusing, we perform a geometric and diffractive study at the focus and compare it to the case of an ellipsoidal mirror used in the same configuration. Indeed the latter is known to be perfectly stigmatic. In both cases, the diffractive approach results in diffraction limited pulses, as depicted in Fig. 9(a-b). Interestingly, the geometric study shows differences between the two situations. In the case of the ellipsoidal mirror, we observe a geometrically perfect focusing to a single point in the spot diagram in Fig. 9(a). In contrast, the focus obtained with the toroidal mirror

#179798 - $15.00 USD Received 13 Nov 2012; revised 21 Dec 2012; accepted 27 Dec 2012; published 25 Jan 2013

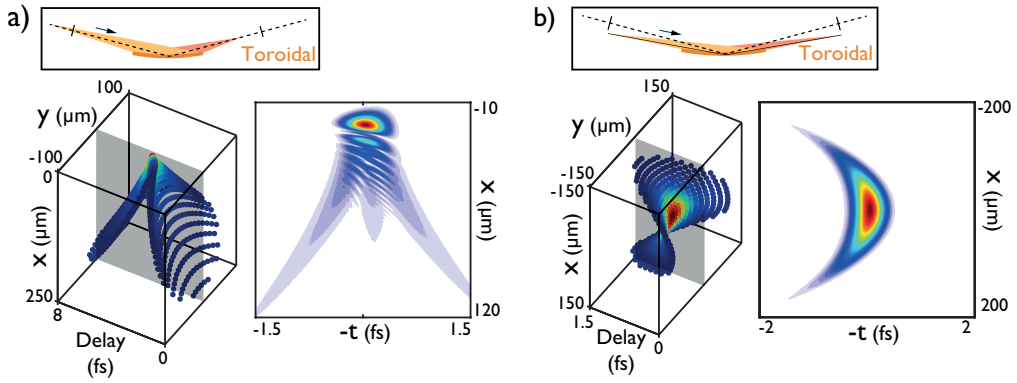

Fig. 10. Detailed evolution of a pulse focused by a toroidal mirror in the case of (a) a 0.5 magnifying power and (b) an error of 0.1° on the grazing angle with a magnification of 1. Upper panel: studied focusing geometry. Left panel: 3D spot diagram. Right panel: evolution of the modulus of the electric field in the $y = 0$ plane, shaded in grey on the 3D spot diagrams.

is deformed by higher-order aberrations, with accumulated delays varying up to 40 as. These complex geometric variations are not visible in the pulse profile obtained by the diffractive approach. Their spatial extension and temporal delays remain smaller than the corresponding diffraction spot size and the chosen pulse duration. Consequently, when decreasing the duration of the initial pulse down to a few tens of attoseconds, the geometric delays would become significant. Moreover, one should keep in mind that the depicted spot diagrams only take into account the rays carrying more than 1% of the maximum flux. We neglect the rays reflected off the periphery of the mirror. On the other hand, if the divergence of the source is increased, the role of the peripheral rays will become significant. In order to illustrate this point, we depict in Fig. 9(c) the 3D spot diagram taking into account the rays coming from the full surface of the mirror, in analogy with Fig. 1(c). The obtained structure is similar to the one depicted in Fig. 9(b), but its dimensions are much larger. The beam has a spatial extension of a few hundreds of microns, and the relative delays between the rays are of several femtoseconds. Thus, the proper use of a toroidal mirror in a $2f-2f$ geometry is subject to several conditions on the pulse duration and the divergence of the source.

In the following focusing geometries, the toroidal and ellipsoidal mirrors will have similar responses. For that reason, we will only treat the case of the toroidal mirror.

It is not always convenient to use a toroidal mirror in a magnification of 1. Consequently, we now consider a magnification of 0.5. As shown in Fig. 8(b) and in more detail in Fig. 10(a), the obtained pulses are distorted by a strong coma aberration inducing the characteristic double pulse front. This focusing geometry is close to the one described in Figs. 1 and 2. More generally, the larger the deviation from the $2f-2f$ geometry, the greater the coma aberration.

In the last case, as depicted in Fig. 8(c), we come back to the $2f-2f$ geometry. We consider the mirror to be set at a grazing angle of 11.4° instead of its optimal value of 11.5°. It becomes obvious that the pulse is distorted by a strong astigmatism, the beam being focused in two orthogonal planes located 25 mm before and after the paraxial focus. Between these two positions, the pulse profile exhibits the well-known saddle-shaped behavior [19]. The same evolution is retrieved with the geometric approach, see Fig. 10(b). In the present case, we chose a deviation of the grazing angle equal to 0.1°. The larger this deviation, the stronger the astigmatism. Therefore, in practice the choice of a focusing optic may not only depend on the magnitude of

#179798 - $15.00 USD Received 13 Nov 2012; revised 21 Dec 2012; accepted 27 Dec 2012; published 25 Jan 2013

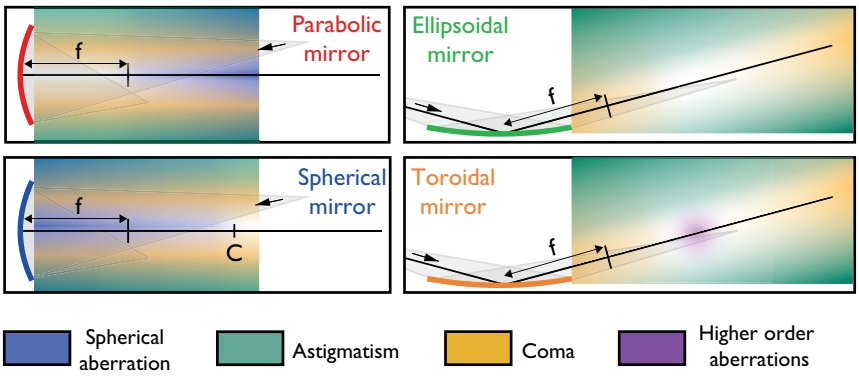

Fig. 11. Summary of the aberrations introduced by the four studied mirrors. The colormap indicates the dominant aberration for a given position of the focal point.

the distortions it induces, but also on its ease of alignment.

In order to summarize the results obtained via the geometric and diffractive approaches, we depict in Fig. 11 an overview of the different aberrations in the studied focusing geometries. The colormap indicates the qualitative strength of the aberrations. However, one should keep in mind that in practice their magnitude strongly depends on the numerical aperture of the beam and the pulse duration. In other words, a loosely focused long pulse will experience weaker spatio-temporal distortions than a tightly focused short pulse.

4. Consequences on the space-time structure and the pulse duration

As a last part of our analysis, we discuss the consequences that aberrations can have on experiments involving attosecond pulses. In order to do so, we use the decomposition of the pulse duration described in Section 2 as a tool to illustrate our discussion.

Among all the obtained spatio-temporal profiles at the focus, one can distinguish three main patterns. The pulse is:

i) either close to the diffraction limit, when focused by a toroidal or ellipsoidal mirror in a $2f-2f$ geometry,

ii) or distorted by a curvature of the pulse front in the presence of spherical aberration or astigmatism,

iii) or split into a double pulse front in the presence of coma.

In Fig. 12, we analyse these situations in more detail. In each case, we depict the spatio-temporal profile of the pulse, its spectral properties in three points, and the decomposition of its duration.

First of all, we consider the pulse being focused by the ellipsoidal mirror in the $2f-2f$ geometry, as described in Fig. 9(a). This case is known to be aberration-free. Thus, the pulse properties are expected to be identical across the beam, as confirmed by Fig. 12(a). When plotting the local spectra and group delays at three points in the beam, it appears that none of these quantities vary in space. Moreover, one can notice the linear increase of the instantaneous frequency and the group delay due to the attochirp. This interpretation is confirmed by the decomposition of the pulse duration. Apart from the bandwidth limit Δt_{FT_G}, the only non-zero contribution is τ_{SP} which represents the variations of the spectral phase. Indeed, the only

#179798 - $15.00 USD Received 13 Nov 2012; revised 21 Dec 2012; accepted 27 Dec 2012; published 25 Jan 2013

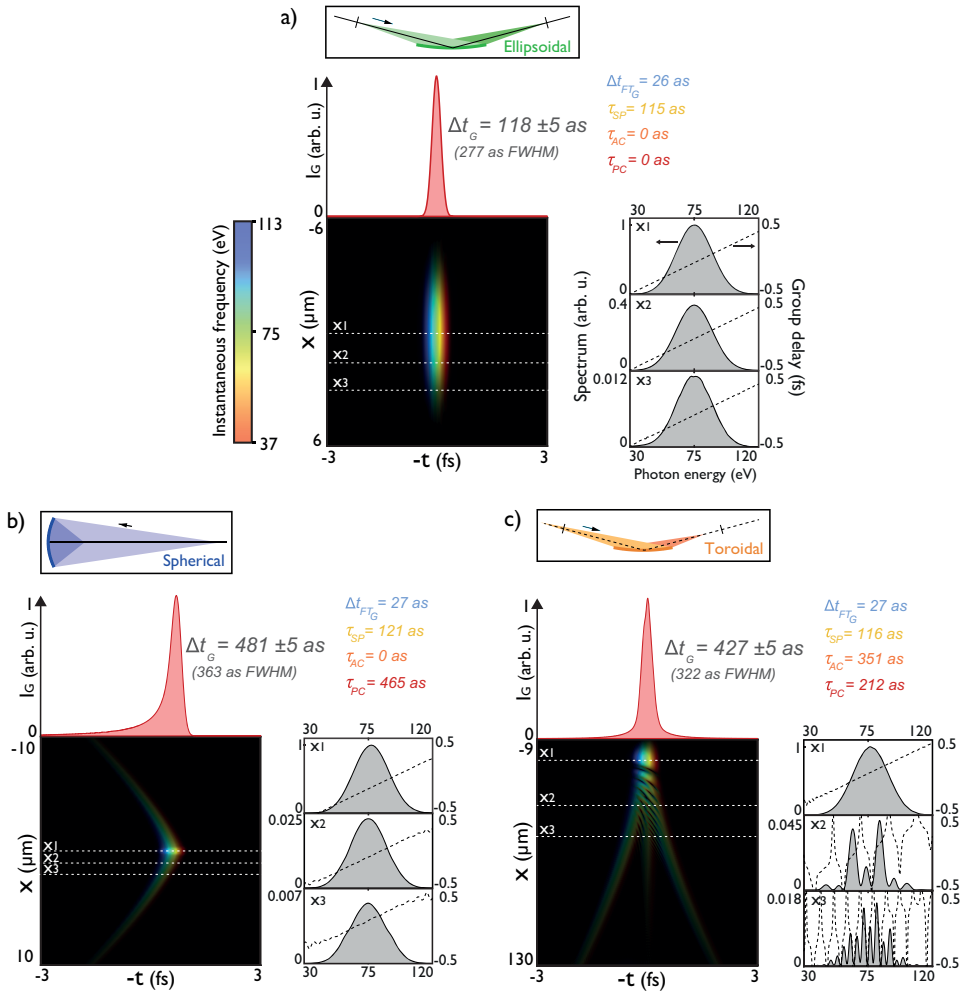

Fig. 12. Decomposition of the global duration of three pulses focused by (a) an ellipsoidal mirror in a $2f-2f$ geometry, (b) a spherical mirror with a zero field angle, and (c) a toroidal mirror with a magnification of 0.5. (a-c) central panel: instantaneous frequency of the pulse in the $y=0$ plane. Lateral panels: local spectra and local group delays at three positions. Upper panel: spatially integrated pulse $I_G(t)$ and its RMS global duration Δt_G, along with its decomposition. $I_G(t)$ and Δt_G are estimated by integrating the full 3D pulse, even though only the pulse in the plane $y=0$ is plotted.

phenomenon increasing the pulse duration is the intrinsic attochirp, which is caused by the generation process itself and is not related to the focusing geometry. If this chirp rate is minimized, the shortest pulse duration and high XUV intensities can be reached, which represents the optimal pulse parameters for experiments.

In the second scenario, we consider the pulse at the paraxial focus of the spherical mirror with zero field angle, as shown in Fig. 7(b). The introduced spherical aberration leads to a curvature of the pulse front. This means that the pulse has the same shape everywhere but exhibits different arrival times across the beam. The spectrum is spatially independent, but the group delay experiences an absolute offset changing in space. The different contributions to the

#179798 - $15.00 USD Received 13 Nov 2012; revised 21 Dec 2012; accepted 27 Dec 2012; published 25 Jan 2013

pulse duration reflect these conclusions. Since at any given point, the local duration remains the same as in the previous situation, Δt_{FT_G} and τ_{SP} do not vary. On one hand, since the shape of the spectrum is independent of space, τ_{AC} has to be zero. On the other hand, since the group delay varies in space, τ_{PC} cannot be zero. Therefore the pulse duration is increased. As a consequence, this could decrease the temporal resolution in attosecond experiments. As an example, such a distortion might lead to a bias when estimating the emission time of electrons released from different atomic shells [8, 9].

Finally, we consider the pulse being focused by a toroidal mirror with a magnification of 0.5. In this geometry, the coma aberration leads to the creation of a double pulse front. Strong oscillations are visible on both the spectrum and the group delay. They originate from spectral interferences between the two time-delayed pulse fronts. Since the spectrum and the group delay are spatially dependent, both τ_{AC} and τ_{PC} are large. In term of applications, we imagine potential issues which could arise with such distortions. For example, when used in pump probe experiments where the attosecond pulse acts as the pump, such a distortion could result in an unwanted double excitation. Also, for spectroscopy experiments which do not require attosecond resolution, but instead make use of the ultrabroad spectrum, the strong modulations of the latter could become problematic. In both cases, this could lead to ambiguities in the interpretation of the obtained data.

One should notice that, with the chosen parameters, the global pulse duration Δt_G is increased up to a factor of 4 compared to the perfect case of the ellipsoidal configuration. This highlights the strong sensitivity of attosecond pulses to aberrations occurring in typical geometries.

5. Conclusion

In conclusion, we presented tools developed to analyze the impact of optical aberrations when focusing attosecond pulses. We used them to study the most common focusing geometries in attosecond experiments, i.e. geometries including parabolic, spherical, toroidal or ellipsoidal mirrors. We have shown that in these geometries, aberrations can lead to important pulse distortions. Moreover, those can be amplified by even small misalignments of the optics. This can significantly deteriorate the pulse properties in space and time, leading to, among others, a decrease of peak intensity and variations of the arrival time of the pulse across the beam.

We considered that a single mirror was used to focus the attosecond pulse, which is mostly the case. However, it would be possible to extend this study to optical systems made of several focusing mirrors. The attosecond pulses would therefore accumulate aberrations of each optic, which would make the alignment of the system even more critical.

In the end, aberrations have a visible impact on the pulse when the induced geometric distortions exceed the diffraction spot size. It is possible to obtain distortion-free pulses by placing an aperture before the mirror, which however implies a reduction of the total flux.

We hope that this study will allow the scientific community to identify potential issues arising when focusing attosecond pulses.

Acknowledgments

We are grateful for the financial support from the Engineering and Physical Sciences Research Council under grants EP/G067694/1 and EP/F034601/1.

#179798 - $15.00 USD Received 13 Nov 2012; revised 21 Dec 2012; accepted 27 Dec 2012; published 25 Jan 2013